

Adiabatic topological passage based on coupling of giant atom with two Su-Schrieffer-Heeger chains

Da-Wei Wang,¹ Ling Zhou,² and Yu-xi Liu^{1,*}

¹*School of Integrated Circuits, Tsinghua University, Beijing 100084, China*

²*School of Physics, Dalian University of Technology, Dalian 116024, China*

We study an adiabatic topological passage of two Su-Schrieffer-Heeger (SSH) chains mediated by a giant atom. When two finite SSH chains are in the topological phase and the frequency of the giant atom is equal to the center frequency of the SSH chains, the system is reduced to a subsystem that describes the coupling of a giant atom to the edge states of two SSH chains. In this case, we can find dark states that act as adiabatic topological passages. This allows us to adiabatically transfer excitations of the giant atom to either one end of two SSH chains in a fully controllable way. In addition, we show good robustness of the adiabatic topological passages to both giant atom frequency mismatch and the coupling disorders in two SSH chains. Our study provides a method to realize quantum information processing and fabricate quantum optical devices based on the coupling of the giant atom to topological matter.

I. INTRODUCTION

A crucial task to implement efficient quantum information processing is information coherent transfer between different nodes [1, 2]. Several quantum channels for state transfer have been proposed in different quantum systems, e.g., optical lattices [3], the systems of cavity quantum electrodynamics [2, 4, 5], photonic and phononic waveguides [6, 7], superconducting quantum circuits [8, 9], quantum dot arrays [10]. However, due to the inevitable environmental effects of these systems, the reliability of quantum information transfer may be significantly reduced. Therefore, how to realize a robust channel for quantum state transfer remains an urgent and ongoing question. Various approaches have been proposed to overcome the effects of perturbations and decoherence during coherent transfer between nodes through the quantum channel, the best-known one is the stimulated Raman adiabatic passage (STIRAP) [11] in a three-levels system [12], in which controllable population transfer between the initial and final states is not subject to any loss of intermediate radiative states [13, 14].

Another option is to utilize topology-protected edge states as quantum channels. One of the most attractive properties of topological systems is that the edge states are robust to small perturbations [15–18]. The research along this direction can be classified into two categories. One is that the information is encoded and processed on the edge states, and the state transfer between two edges is realized via well-known adiabatic techniques [19–22], Landau-Zener tunnel [21] or STIRAP [11, 23, 24]. These methods are well adapted to non-diagonal disorder, but the speed of the state transfer is intrinsically limited by the adiabatic requirements, i.e., avoiding unwanted adiabatic transitions in the edge states. The Su-Schrieffer-Heeger (SSH) model and its various extensions have been investigated in this scenarios [9, 22, 25–29]. Beyond the

fast and robust quantum state transfer based on topological edge state channels, a large amount of work has been devoted to study topological quantum devices for robust information processing, e.g., topological beam splitters, routers and other combinations [30–33]. Another topology-based channel is to couple the quantum system with topological systems, in which their couplings are manipulated to realize topology-preserving quantum information processing [27, 34–41]. For example, a topologically protected channel has been proposed for quantum state transfer between remote quantum nodes, in which the quantum state transfer is mediated by edge modes of a chiral spin liquid, and this method is intrinsically robust to realistic defects associated with disorder and decoherence [38].

Recently, giant atoms have been studied [42–45] for coupling them to can be to the waveguide via several different coupling points. This results in many interesting phenomena, such as frequency-dependent decay rates and Lamb shifts [46, 47], decoherence-free interaction [48–50], chiral phenomena [51, 52], oscillating bound states [53, 54], and non-Markovian effects [42, 55, 56]. These new phenomena arise from the interference and time-delay effects of the electromagnetic fields propagating between coupling points. In addition, the giant atom can also be coupled to several waveguides for implementing controllable transmission of photons between different waveguides [57]. Here, we consider a giant atom, which is coupled to two finite SSH chains. We propose to realize directional quantum state transfer by constructing the adiabatic topological passage. When the two finite SSH chains are in topological phase, the whole system is reduced to a subsystem that describes the coupling of a giant atom to the edge states of two SSH chains. Then, the subsystem can be equivalently described by a five-state model consisting of the edge states of the two SSH chains as well as the giant atom. In this case, we find that there is a dark state in the subsystem that can act as an adiabatic topological passage, allowing us to adiabatically transfer the excited state of the giant atom to

* yuxiliu@mail.tsinghua.edu.cn

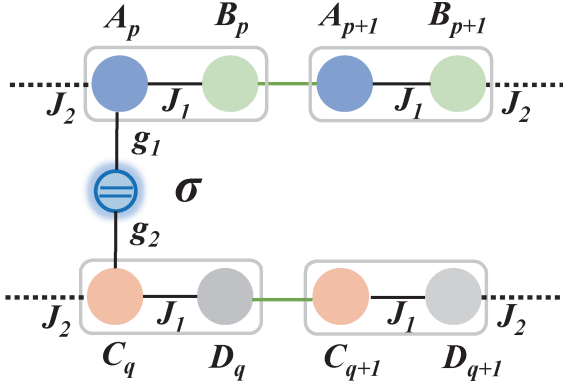


FIG. 1. Schematic diagram for the coupling of a giant atom to two finite SSH chains at sublattice A_p and C_q with coupling strength g_1 and g_2 , respectively. Alternatively, the giant atom can also be coupled to the sublattice B_p or D_q (not shown here).

either end of the two SSH chains in a fully controllable way. Moreover, we discuss the effects of the giant atom frequency mismatch and non-diagonal disorder in SSH chains, and the results show that our proposal exhibits good robustness to both of these imperfections.

The paper is organized as follows: In Sec. II, we describe a theoretical model and derive the effective Hamiltonian for realizing the coupling between giant atom and edge states of the two SSH chains. In Sec. III, We construct adiabatic topological passages and apply them to quantum information transfer. In Sec. IV, we discuss the imperfection effect on the adiabatic topological passages. In Sec. V, we further discuss our result and experimental feasibility. Finally, we conclude our results in Sec. VI.

II. ATOM COUPLING WITH THE FINITE SSH CHAIN

As schematically shown in Fig. 1, we consider the system that a two-level giant atom is coupled to two finite SSH chains denoted by SSH-1 and SSH-2, respectively. The giant atom is coupled to the SSH-1 chain via either the sublattice A_p or the sublattice B_p of the p th cell with the coupling strength g_1 . However, the coupling to the SSH-2 chain is realized via either sublattice C_p or the sublattice D_p of the q th cell with the coupling strength g_2 . The total Hamiltonian can be written as

$$H = \omega_e \sigma^\dagger \sigma^- + H_{\text{SSH}}^1 + H_{\text{SSH}}^2 + [(g_1 x_p^\dagger + g_2 y_q^\dagger) \sigma + \text{h.c.}], \quad (1)$$

where $\sigma^\dagger = |e\rangle\langle g|$ and $\sigma^- = |g\rangle\langle e|$ are the raising and lowering operators of the giant atom with the frequency ω_e from the ground $|g\rangle$ to the excited $|e\rangle$ state. The operator $x_p^\dagger = a_p^\dagger$ or b_p^\dagger ($y_q^\dagger = c_q^\dagger$ or d_q^\dagger) represents the creation operator in the sublattice A_p or B_p (C_q or D_q) with the possible coupling of the giant atom to the SSH-1

(SSH-2) chain. There are four possible coupling scenarios $(a_p^\dagger, c_q^\dagger)$, $(a_p^\dagger, d_q^\dagger)$, $(b_p^\dagger, c_q^\dagger)$ and $(b_p^\dagger, d_q^\dagger)$. For example, the scenario $(a_p^\dagger, c_q^\dagger)$ denotes that the giant atom is coupled to the sublattice A_p of the p th cell of the SSH-1 chain and the sublattice C_q of the q th cell of the SSH-2 chain. The Hamiltonians H_{SSH}^1 and H_{SSH}^2 in Eq. (1) corresponding to two SSH chains are

$$H_{\text{SSH}}^1 = \sum_{i=1}^N \omega_o (a_i^\dagger a_i + b_i^\dagger b_i) + (J_1 a_i^\dagger b_i + J_2 a_{i+1}^\dagger b_i + \text{h.c.}), \quad (2a)$$

$$H_{\text{SSH}}^2 = \sum_{i=1}^N \omega_o (c_i^\dagger c_i + d_i^\dagger d_i) + (J_1 c_i^\dagger d_i + J_2 c_{i+1}^\dagger d_i + \text{h.c.}). \quad (2b)$$

Here, we assume that all sublattices have the same frequency ω_o such that the quantized Zak phase in the SSH model is still valid [58, 59]. We define ω_o as the central frequency of the SSH chains and consider it as the reference in the following discussions. The intra-cell sublattice jump and inter-cell sublattice hopping strengths in the SSH-1(SSH-2) chain are $J_1 = J(1 + \cos\theta)$ and $J_2 = J(1 - \cos\theta)$ with $\theta \in [0, 2\pi]$, respectively. For the finite-sized SSH chain, when the hopping strength of the SSH model satisfies $J_1 > J_2$, the SSH model is in the trivial phase, in this case, there exists only one finite energy gap in the energy spectrum; when the hopping strength satisfies $J_1 < J_2$, the SSH model is in the topological phase in which there exists two degenerate states in the energy gap, arising from the hybridization of the left and right edge states due to finite-size effects [60]. These two band-gap states are topology-protected, and thus utilizing topology-protected states to transfer information may be robust to a certain range of disorders.

In the single-excited space, we label $|A_i\rangle = a_i^\dagger|G\rangle$ and $|B_i\rangle = b_i^\dagger|G\rangle$ ($|C_i\rangle = c_i^\dagger|G\rangle$ and $|D_i\rangle = d_i^\dagger|G\rangle$), where $|G\rangle$ is the ground state of the SSH-1 (SSH-2) chain. We can diagonalize the Hamiltonian in Eqs. (2a) and (2b) as $H_{\text{SSH}}^1 = \sum_{j=1}^{2N} E_j |\Psi_j\rangle\langle\Psi_j|$, where E_j and $|\Psi_j\rangle$ are the eigenenergies and corresponding eigenvectors with $E_{2N} > E_{(2N-1)} > \dots > E_1$; $H_{\text{SSH}}^2 = \sum_{j=1}^{2N} \varepsilon_j |\Phi_j\rangle\langle\Phi_j|$ with the eigenenergies ε_j and the eigenvectors $|\Phi_j\rangle$ with $\varepsilon_{2N} > \varepsilon_{(2N-1)} > \dots > \varepsilon_1$. It can be verified that $E_N \approx E_{N+1} \approx \varepsilon_N \approx \varepsilon_{N+1} \approx 0$ in the topological phase for the finite length of the chains when ω_o is taken as the reference energy. For scenario $(a_p^\dagger, c_q^\dagger)$, we can rewrite the Hamiltonian (1) as

$$H = \Delta \sigma^\dagger \sigma^- + \sum_{j=1}^{2N} [E_j |\Psi_j\rangle\langle\Psi_j| + \varepsilon_j |\Phi_j\rangle\langle\Phi_j| + (g_1 \eta_{2p-1,j} \Psi_j^\dagger + g_2 \zeta_{2q-1,j} \Phi_j^\dagger) \sigma^- + \text{h.c.}], \quad (3)$$

with $\Delta = \omega_e - \omega_o$, $\Psi_j^\dagger = |\Psi_j\rangle\langle G|$ and $\Phi_j^\dagger = |\Phi_j\rangle\langle G|$. $g_1 \eta_{2p-1,j} = g_1 \langle\Psi_j|A_p\rangle$ ($g_2 \zeta_{2q-1,j} = g_2 \langle\Phi_j|C_q\rangle$) is the

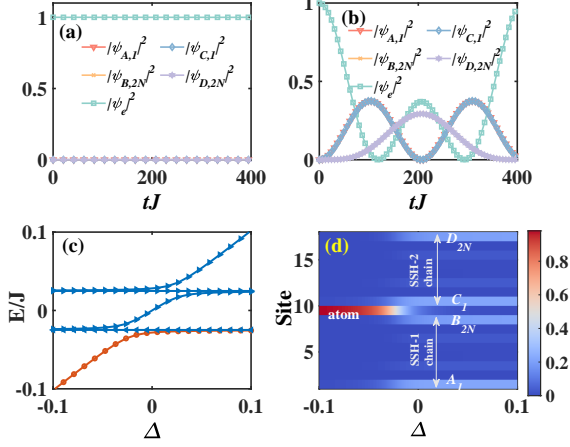


FIG. 2. The probability evolution of the atomic excited state $|\psi_e|^2$, sublattice A_1 ($|\psi_{A,1}|^2$), sublattice B_{2N} ($|\psi_{B,2N}|^2$), sublattice C_1 ($|\psi_{C,1}|^2$) and sublattice D_{2N} ($|\psi_{D,2N}|^2$) with $\Delta = 0$ for (a) $\theta = 0.4\pi$ (trivial phase) and for (b) $\theta = 0.7\pi$ (topological phase). (c) The partial energy spectrum of the system varies with Δ for the two SSH chains in the topological phase. (d) The distribution of the probability of hybridized mode that the circle marker in panel (c) varies with Δ . The parameters are $p = q = 1$, $N = 4$, $g_1 = g_2 = 0.01J$ and $J = 1$.

coupling strength between the giant atom and the SSH-1 (SSH-2) chain in the diagonalized basis. Hereafter, $g_1\eta_{2p-1,j}$ (or $g_1\eta_{2p,j}$) is the coupling strength when the giant atom is coupled to the sublattice A (or B) of the p th unit cell in the SSH-1, and $g_2\eta_{2q-1,j}$ (or $g_2\eta_{2q,j}$) is the coupling strength when the giant atom is coupled to the sublattice C (or D) of the q th unit cell in the SSH-2.

In the interaction picture by performing the unitary transformation

$$U = \exp \left[-i \left(\sum_{j=1}^{2N} E_j \Psi_j^\dagger \Psi_j + \varepsilon_j \Phi_j^\dagger \Phi_j + \Delta \sigma^\dagger \sigma^- \right) t \right], \quad (4)$$

the Hamiltonian (3) can be written as

$$H_I = \sum_{j=1}^{2N} \left[g_1 \zeta_{2p-1,j} e^{i(E_j - \Delta)t} \Psi_j^\dagger \sigma^- + g_2 \eta_{2q-1,j} e^{i(\varepsilon_j - \Delta)t} \Phi_j^\dagger \sigma^- + \text{h.c.} \right]. \quad (5)$$

Below, we consider that the giant atom resonantly interacts with the SSH-1 and SSH-2 chains with $\Delta = 0$ and the condition $\{g_1/J, g_2/J\} \ll 1$. For the SSH-1 and SSH-2 chains in the trivial phase, the giant atom nearly decouples from the chain due to $|E_j| \gg g_1$ and $|\varepsilon_j| \gg g_2$. In Fig. 2(a), we plot the dynamical evolution of the system when the system is initially in the excited state $|e\rangle$ of the giant atom and the vacuum state of the two SSH chains with $\theta = 0.4\pi$. It can be found that the excitation remains in the atom and is not exchanged with two SSH chains. For the SSH-1 and SSH-2

chains in the topological phase, due to the presence of four band-gap states corresponding to nearly zero energy $\{E_N, E_{N+1}, \varepsilon_N, \varepsilon_{N+1}\} \approx 0$, which are near resonant with the atomic frequency for $\Delta = 0$, then the coupling between other eigenstates and the giant atom can be neglected due to $|E_j| \gg g\eta_{2p-1,j} > 0$ and $|\varepsilon_j| \gg g\zeta_{2q-1,j}$ for $j \neq N, N+1$. Under this case, the effective interaction Hamiltonian of the giant atom and the SSH chains in the Schrödinger's picture can be written as

$$\begin{aligned} H = & E_N \Psi_N^\dagger \Psi_N + E_{N+1} \Psi_{N+1}^\dagger \Psi_{N+1} \\ & + \varepsilon_N \Phi_N^\dagger \Phi_N + \varepsilon_{N+1} \Phi_{N+1}^\dagger \Phi_{N+1} \\ & + [g_1(\eta_{2p-1,N} \Psi_N^\dagger + \eta_{2p-1,N+1} \Psi_{N+1}^\dagger) \sigma^- \\ & g_2(\zeta_{2q-1,N} \Phi_N^\dagger + \zeta_{2q-1,N+1} \Phi_{N+1}^\dagger) \sigma^- + \text{h.c.}]. \end{aligned} \quad (6)$$

That is, in the single-excitation space, when we consider that the giant atom is resonant with the SSH chain, the above Hamiltonian only causes the following subspace transitions $\{|\psi_N, g\rangle, |\phi_N, g\rangle\} \leftrightarrow |vac, e\rangle \leftrightarrow \{|\psi_{N+1}, g\rangle, |\phi_{N+1}, g\rangle\}$. We also plot the dynamical evolution of the system in Fig. 2(b) with the same parameters as in Fig. 2(a) except $\theta = 0.7\pi$. We can find that the excited state of the giant atom can be transferred to the end lattices of the two SSH chains. We have also plotted the energy spectrum of the system corresponding to the Hamiltonian in Eq. (1) with the variation of the detuning Δ in Fig. 2(c), where we show only the range of $E \in [-0.1J, 0.1J]$ to see the details clearly. In this energy range, there are only five energy levels. It can be seen that the energy levels show an anti-crossing property. That is, there are coherent couplings [61, 62] between the giant atom and two SSH chains, and the giant atom is coupled to the band-gap states in the two SSH chains. In Fig. 2(d), the probability distribution of the hybridization mode on the sites is plotted with the variation of Δ . One can see that the contribution of the hybridization mode gradually varies from the giant atom to the two SSH chains with the increase of Δ . It also shows that an effective transition between the giant atom and the SSH chain exists.

For an SSH chain in the topological phase, there are two band-gap states, which are the hybridization of the left and right edge states due to finite size effects [60] of the chain. The energies of two band-gap states can be calculated as $E_N = -E_{N+1} = N_L^2(-1)^{N+1} J_1(J_1/J_2)^{N-1}$ ($\varepsilon_N = -\varepsilon_{N+1} = N_L^2(-1)^{N+1} J_1(J_1/J_2)^{N-1}$) and the corresponding wavefunction can be written as [60]

$$\begin{aligned} |\Psi_N\rangle &= \frac{1}{\sqrt{2}}(|\psi_L\rangle + |\psi_R\rangle), |\Psi_{N+1}\rangle = \frac{1}{\sqrt{2}}(|\psi_L\rangle - |\psi_R\rangle), \\ |\Phi_N\rangle &= \frac{1}{\sqrt{2}}(|\varphi_L\rangle + |\varphi_R\rangle), |\Phi_{N+1}\rangle = \frac{1}{\sqrt{2}}(|\varphi_L\rangle - |\varphi_R\rangle), \end{aligned} \quad (7)$$

where $|\psi_L\rangle = N_L \sum_{i=1}^N \alpha_i^a |A_i\rangle$ ($|\varphi_L\rangle = N_L \sum_{i=1}^N \alpha_i^c |C_i\rangle$) with $\alpha_i^{a/c} = (-J_1/J_2)^{i-1}$ and $|\psi_R\rangle = N_R \sum_{i=1}^N \alpha_i^b |B_i\rangle$ ($|\varphi_R\rangle = N_R \sum_{i=1}^N \alpha_i^d |D_i\rangle$) with $\alpha_i^{b/d} = (-J_1/J_2)^{N-i}$ are

the left and right edge states of the SSH-1 (SSH-2) chain. $N_L = N_R = [1 - (J_1/J_2)^2]^{1/2} [1 - (J_1/J_2)^{2N}]^{-1/2}$ are the normalization constants. Using Eq. (7), we can calculate the coupling strength of the giant atom to the SSH chains in the diagonalized basis as $g_1 \eta_{2p-1, N} = -g_1 \eta_{2p-1, N+1} = g_1 c_p^a / \sqrt{2}$ and $g_2 \zeta_{2q-1, N} = -g_2 \zeta_{2q-1, N+1} = g_2 c_q^c / \sqrt{2}$.

In the same way, we can obtain the effective coupling strengths of the giant atom to the sublattices B_p and D_q respectively as $g_1 \eta_{2p, N} = -g_1 \eta_{2p, N+1} = g_1 c_p^b / \sqrt{2}$ and $g_2 \zeta_{2q, N} = -g_2 \zeta_{2q, N+1} = g_2 c_q^d / \sqrt{2}$. We can see that these couplings depend on the coupling positions of the giant atom to the chains. For example, for $\eta_{2p-1, N} = (-J_1/J_2)^{p-1} \sqrt{2}$, it decreases as p increases when $J_1 < J_2$, while $\eta_{2p, N} = (-J_1/J_2)^{N-p} / \sqrt{2}$ increases with the increase of p . Then, the effective coupling strength of the giant atom to the SSH chains can be adjusted by changing the coupling position.

III. DIRECTIONAL AND CONTROLLABLE EXCITATION TRANSFER THROUGH THE ADIABATIC PROCESS

Now, substituting Eq. (7) into Eq. (5), the effective interaction Hamiltonian between two the SSH chains in the topological phase and giant atom can be rewritten as

$$H_{sub} = G|\psi_L, g\rangle\langle\psi_R, g| + G|\varphi_L, g\rangle\langle\varphi_R, g| + G_{L,a}|\psi_L, g\rangle\langle vac, e| + G_{L,c}|\varphi_L, g\rangle\langle vac, e| + \text{h.c.}, \quad (8)$$

in the subspace $\{|vac, e\rangle, |\psi_L, g\rangle, |\psi_R, g\rangle, |\varphi_L, g\rangle, |\varphi_R, g\rangle\}$, where $G = (-1)^{N+1} N_L^2 J_1 (J_1/J_2)^{N-1}$ is the hybridization coupling strength between the left and right edge states due to finite size effects. $G_{L,a} = g_1 N_L (-J_1/J_2)^{p-1}$ and $G_{L,c} = g_2 N_L (-J_1/J_2)^{q-1}$ are the effective coupling strengths between the giant atom and two SSH chains and decay with the power exponent of p and q , respectively. The energy state transitions described in Eq. (8) are shown schematically in Fig. (3).

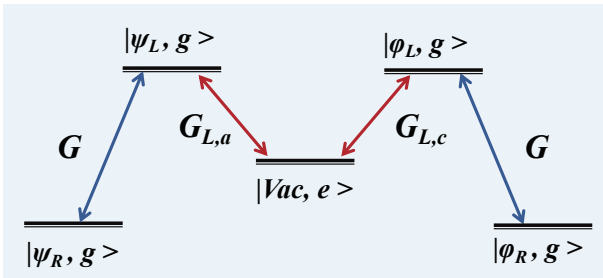


FIG. 3. Schematic diagram of the transition of the subspace states $\{|vac, e\rangle, |\psi_L, g\rangle, |\psi_R, g\rangle, |\varphi_L, g\rangle, |\varphi_R, g\rangle\}$.

We can find that the giant atom is equivalently coupled to the left edge states $|\psi_L, g\rangle$ and $|\varphi_L, g\rangle$ when the giant atom is coupled to the sublattices A_p and C_q . Thus, we can conclude that when the giant atom is resonantly coupled to the two SSH chains in the topological phase,

the full system containing the giant atom and two SSH chains can be reduced to a five-state model. And, the coupling of the giant atom to edge states provides us with a way to manipulate edge states through an atom. Rewriting Eq. (8) in the matrix form, we can obtain

$$H_{sub} = \begin{bmatrix} 0 & G_{L,a} & 0 & G_{L,c} & 0 \\ G_{L,a} & 0 & G & 0 & 0 \\ 0 & G & 0 & 0 & 0 \\ G_{L,c} & 0 & 0 & 0 & G \\ 0 & 0 & 0 & G & 0 \end{bmatrix}. \quad (9)$$

By using the eigenvalue equation corresponding to the Hamiltonian H_{sub} in Eq. (9)

$$\lambda(\lambda^2 - G^2)[\lambda^2 - (G^2 + G_{L,a}^2 + G_{L,c}^2)] = 0, \quad (10)$$

we can obtain 5 eigenvalues $\lambda_0 = 0$, $\lambda_{\pm 1} = \pm G$ and $\lambda_{\pm 2} = \pm \sqrt{G^2 + G_{L,a}^2 + G_{L,c}^2}$. We can also obtain the eigenstate corresponding to the eigenvalue $\lambda_0 = 0$ as

$$|\Psi_0\rangle = \{\cos \chi; 0; \sin \chi \cos \phi; 0; \sin \chi \sin \phi\}, \quad (11)$$

where $\tan \chi = \sqrt{G_{L,a}^2 + G_{L,c}^2} / G$ and $\tan \phi = G_{L,c} / G_{L,a}$ are the mixing angles. It can be seen that the zero-energy eigenstate $|\Psi_0\rangle$ is a superposition of the atomic excited states (with probability $\cos^2 \chi$), the right edge state of the SSH-1 chain (with probability $\sin^2 \chi \cos^2 \phi$) and the right edge state of the SSH-2 chain (with probability $\sin^2 \chi \sin^2 \phi$). Actually, the zero-energy eigenstate $|\Psi_0\rangle$ is the so-called dark state or coherent population trapping state, and the adiabatic evolution of the zero energy state is analogous to the stimulated Raman adiabatic passage process [11]. However, two topological states are involved, thus we here call this adiabatic process as the adiabatic topological passage.

Let us assume that $\theta(t) = \Omega t$ is time-dependent with rate Ω , then the couplings become $J_1 = J(1 + \cos \Omega t)$ and $J_2 = J(1 - \cos \Omega t)$. The time-dependent mixing angles can be obtain $\chi(t) = \arctan(\sqrt{G_{L,a}^2(t) + G_{L,c}^2(t)} / G(t))$ and $\phi = \arctan(G_{L,c}(t) / G_{L,a}(t))$. In Fig. 4(a), we plot the variation of $\chi(t)$ with $\theta(t)$ for $q = 4$ and different p . It can be found that $\chi(t)$ changes from $\chi(t) = 0$ to $\chi(t) = \pi/2$ as $\theta(t)$ increases, implying that the atomic excited state is transferred to the right edge states of the SSH-1 and SSH-2 chains. Moreover, the reason that the transfer time depends on the atomic coupling position p is that when we choose $q = 4$, $G_{L,c}^2(t)$ will be close to 0, and then as p is increased, $\chi(t)$ becomes small for a fixed $\theta(t)$, and the corresponding state transfer time also increases. As for $q = 1$, one can show that the transfer time is independent of p , which we don't show here. For $\tan \phi = G_{L,a} / G_{L,c}$, it can be simplified as $\tan \phi = g_2 / g_1 (-J_1/J_2)^{q-p}$. Obviously, ϕ is a constant for $g_1 = g_2$ and $p = q$. For $g_2 = g_1$, we find that ϕ eventually

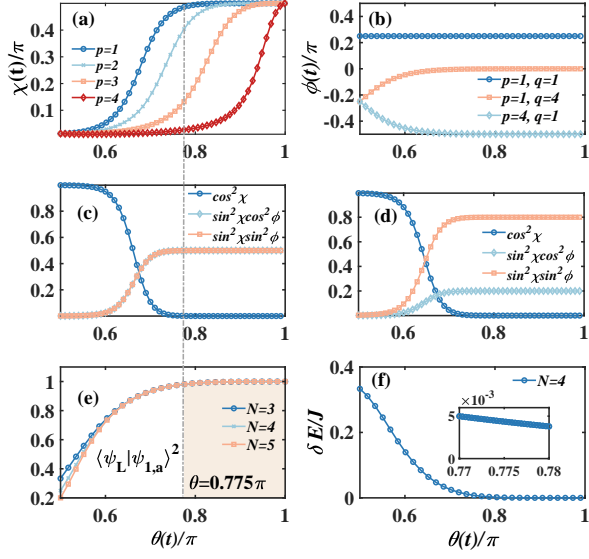


FIG. 4. (a) Mixing angle $\chi(t)$ as a function of $\theta(t)$ for $q = 4$ and different p . (b) Mixing angle $\phi(t)$ vary with θ for $p = q = 1$ (circle), $p = 1, q = 4$ (square), and $p = 4, q = 1$ (diamond). The parameter $g_1 = g_2 = 0.01J$ for panels (a-b). The probability distribution of the zero energy state in giant atomic excited state (circle), right edge state of SSH-1 chain (diamond), and right edge state of SSH-2 chain (square) versus $\theta(t)$ with $p = q = 1$ for $g_2 = 0.01J$ (c) and $g_2 = 0.02J$ (d), respectively; for both (c) and (d) $g_1 = 0.01J$. For panel (a-d) $N = 4$. (e) The distribution of the probability that the right edge state of SSH-1 chain is in the rightmost sublattice A_1 for different N . (f) The energy level difference δE varies with $\theta(t)$.

approaches 0 with the increase of the evolution time t when $p < q$ and $-\pi/2$ when $p > q$ as shown in Fig. 4(b). Because the distribution of probabilities of the two right edge states is proportional to $\tan^2 \phi$, thus we can adjust the coupling positions between the giant atom and the SSH chains to change such distribution. For example, if $p = 1, q = 4$, then $\phi(t) = 0$ at the end of transfer time. This means that the excitation of the giant atom is only transferred to the right edge state of the SSH-1 chain and the SSH-2 chain is always in the vacuum state.

More particularly, if $p = q$, then $\tan^2 \phi = g_2^2/g_1^2$, the transfer of atomic excitations to the right edge states of the two SSH chains depends only on the ratio between the atom-chain coupling strengths. In Figs. 4(c) and (d), we display the probability distribution of the zero energy state in giant atomic excited state (circle), right edge state of SSH-1 chain (diamond), and right edge state of SSH-2 chain (square) versus $\theta(t)$ for $g_2 = 0.01J$ and $g_2 = 0.02J$, respectively. We can see that the probability of the right state of two SSH chains is proportional to the coupling modulus. Furthermore, with the variation of $\theta(t)$ from $\pi/2$ to π , the probability of the right edge state $|\psi_R\rangle$ for the SSH-1 chain is mainly dis-

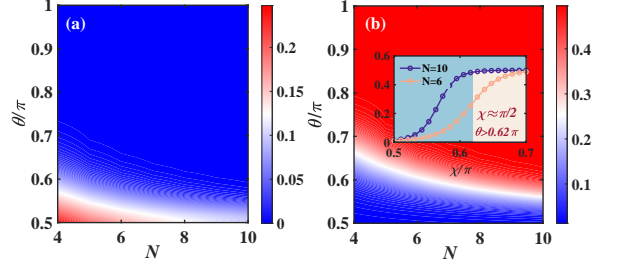


FIG. 5. $|G|$ in (a) and χ/π in (b) as a function of N and θ . The inset of the panel (b) shows χ varying with θ for $N = 6, 10$. The parameters are $g_1 = g_2 = 0.01J$, $\Delta = 0$ and $J = 1$.

tributed on the right sublattice B_{2i} , and is eventually distributed on the rightmost sublattice B_{2N} when $\theta(t)$ is up to $\theta(t) = 0.775\pi$ as shown in Fig. 4(e). In addition, the transfer time from the right edge state to B_{2N} is independent of N . Combining with Figs. 4(c-e), we can conclude that the giant atomic excitations can be transferred to the rightmost sublattices B_{2N} or D_{2N} of the two SSH chains by adjusting $\theta(t)$.

It is essential to note that the entire process needs to be adiabatic. In order to assure the adiabatic evolution, we introduce the adiabaticity parameter [14]

$$\Lambda(t) = \left| \frac{\langle \dot{\Psi}_G | \Psi_0 \rangle}{\lambda_1(t) - \lambda_0(t)} \right|, \quad (12)$$

where $|\Psi_G\rangle$ is the eigenstate corresponding to eigenvalue λ_{+1} . For adiabatic evolution, the key requirement is that $\Lambda(t) \ll 1$ throughout the evolution, which suppresses the transition from $|\Psi_0\rangle$ to $|\Psi_G\rangle$ during the evolution. In other words, this condition is equivalent to the fact that the zero-energy state $|\Psi_0\rangle$ and its nearest-energy state $|\Psi_G\rangle$ are not degenerate during the time evolution. Therefore, we only need to make sure that there is no level crossing after the excitation is transferred from the atom to the right edge states.

In Fig. 4(f), we plot the difference between the zero-energy and the nearest energy labeled as $\delta E = \lambda_{+1(t)} - \lambda_0(t) = G$ for different N . We can see that for $N = 4$, $\delta E > 10^{-3}$ when $\theta(t) = 0.775\pi$ shown in the inset of Fig. 4(f), which means that the energy levels are not degenerate and satisfy the adiabatic evolution. We also discuss whether large N allows us to utilize adiabatic evolution. Combined with the above analysis, for a given number N , the adiabatic evolution is valid as long as $|G| \neq 0$ can be guaranteed during the slow change of θ . In Fig. 5(a), we display the energy difference $\delta E = |G|$ as a function of N and θ . One can see that $|G|$ decreases as N and θ increase. Meanwhile, χ as a function of N and θ is shown in Fig. 5(b). It can be found that χ gradually approaches $\pi/2$ with the increase of θ and N . This implies the change of the probability distribution for the zero-energy state in Eq. (11) from the giant atom to the edge states of the SSH chains. In the inset of

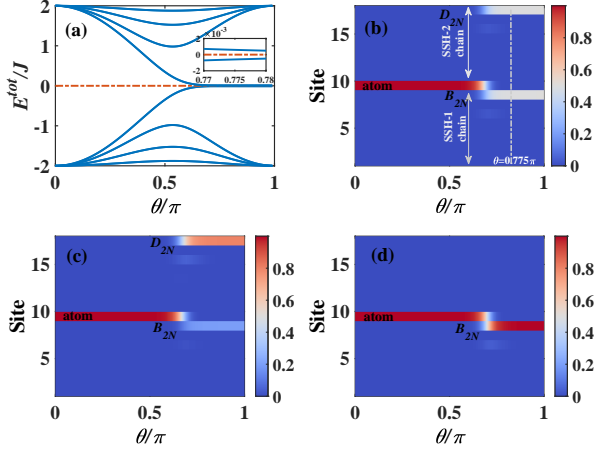


FIG. 6. (a) The energy spectrum of the total Hamiltonian in Eq. (1) with the variation of θ when the giant atom is coupled to the sublattices A_1 and C_1 . (b) The probability distribution of the zero energy state of the panel (a) with orange dashed line on the sites varies with θ . [(c), (d)] The probability distribution of the zero energy state on the sites varies with θ for the parameters $g_1 = 0.01J$, $g_2 = 0.02J$, $p = 1$, $q = 1$ (c); $g_1 = g_2 = 0.01J$ and $p = 1, q = 4$ (d), respectively. The parameters are set to $N = 4$ and $J = 1$ for all figures.

Fig. 5(b), we display variation of χ with θ for $N = 10$. The results show that χ is approached more quickly as $\pi/2$ when $N = 10$ compared to $N = 6$.

In order to prove the correctness of the five-state model, in Fig. 6(a), we plot the variation of energy spectrum E_j^{tot} ($j = 1, \dots, 4N + 1$) corresponding to the total Hamiltonian in Eq. (1) with the change of θ under the case that the giant atom is coupled to the sublattices A_p and C_q . It can be found that there exists a zero-energy state $|E_{2N+1}^{tot}\rangle$ within $\theta = [0, \pi]$. In Fig. 6(b), we plot the probability distribution of $|E_{2N+1}^{tot}\rangle$ on the sites varying with θ . We find that in the range $\theta \in [0, 0.5\pi]$, the probability distribution of $|E_{2N+1}^{tot}\rangle$ is concentrated on the giant atom, which is consistent with Fig. 2(c), where there is no transition between giant atom and SSH chains. With changing θ into topological phase, the giant atom interacts with SSH chains and the component of zero-energy state $|E_{2N+1}^{tot}\rangle$ gradually changes from the giant atom to the rightmost sublattice B_{2N} of SSH-1 chain and sublattice D_{2N} of SSH-2 chain with the same probability as θ increases. Furthermore, we can see that at $\theta = 0.775\pi$ (white line) the atomic excitations have been transferred to the edge states of two SSH chains, but the energy levels are still separated [see inset in Fig. 6(a)], thus the requirement for adiabatic evolution is satisfied for Eq. (12). We also plot the case for $g_2/g_1 = 2$ and $p = q = 1$ in Fig. 6(c). The results also show the probability distribution of the two right edge states, depending on the modulus of the coupling strength between the atom and the SSH-1(2) chain, which coincides with Figs. 4(c) and

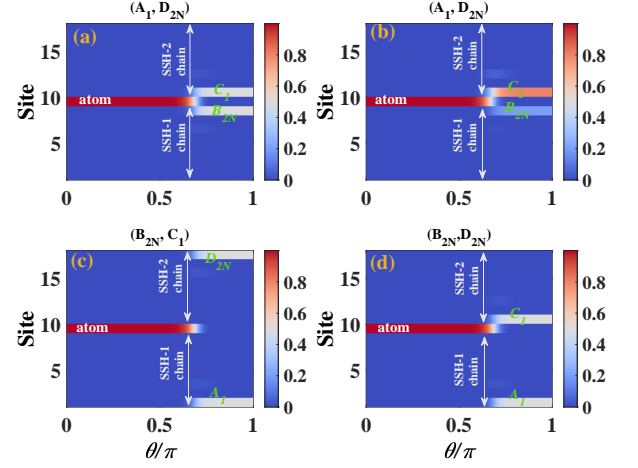


FIG. 7. [(a)-(d)] The transfer of the atomic excitation for the coupling cases (a) and (b) ($a_1^\dagger, d_{2N}^\dagger$); (c) ($b_{2N}^\dagger, c_1^\dagger$) and (d) ($b_{2N}^\dagger, d_{2N}^\dagger$). The parameters are $\Delta = 0$, $J = 1$ and $g_1 = g_2 = 0.01J$ except $g_1 = 0.01J, g_2 = 0.02J$ for the panel (b).

(d) obtained from Eq. (9). In Fig. 6(d), we consider that the giant atom is coupled to different cells of two SSH chains such as $p = 1, q = 4$ with $g_2/g_1 = 1$. We can see that the probability distribution of the zero-energy state transfers from the giant atom only to the right edge state of the SSH-1 chain and eventually to the rightmost sublattice B_{2N} . With the same coupling strength $g_1 = g_2$, the transfer to the rightmost sublattices B_{2N} and D_{2N} of the SSH-1(2) chain can be realized by controlling the atomic coupling positions p and q . Meanwhile, for $p = q$, we can determine the probability of information transfer to B_{2N} and D_{2N} by adjusting g_2/g_1 the ratio of the coupling. Therefore, the zero-energy state obtained in subspace in Eq. (8) is equivalent to the zero-energy state obtained in full Hamiltonian in Eq. (1), which means that we can construct adiabatic topological passages that allow the excitation of a giant atom to be delivered in a controlled way towards the ends of the two SSH chains.

We also plot the component distribution of zero energy state $|E_{2N+1}^{tot}\rangle$ corresponding to the other coupling cases ($a_1^\dagger, d_{2N}^\dagger$), ($b_{2N}^\dagger, c_1^\dagger$) and ($b_{2N}^\dagger, d_{2N}^\dagger$). As shown in Figs. 7(a) and (b), we consider the coupling of the giant atom to the two SSH chains via sublattices A_1 and D_{2N} with the coupling strength $g_1 = g_2 = 0.01J$ and $g_1 = 0.01J, g_2 = 0.02J$, respectively. It can be found that the zero-energy state probability distribution gradually transfers from the giant atom to the rightmost sublattice of the SSH-1 chain B_{2N} and the leftmost sublattice of the SSH-2 chain C_1 . Meanwhile, the excitation occupancy in B_{2N} and C_1 also depends on the square of the ratio g_2/g_1 of couplings. For the remaining two coupling scenarios, we also display them in Figs. 7(c) and (d). Therefore, we can conclude that when giant atom is coupled to the two SSH chains, there will exist a zero-energy state of the sys-

tem, whose distribution is dominated by giant atom when the two SSH chains are in the trivial phase. With the adjustment of θ , the two SSH chains enter the topological phase, and the distribution of the zero energy state will be gradually transferred to the end of the two SSH chains. The end probabilities of the two SSH chains can be adjusted by adjusting the coupling strength of the atoms to the two SSH chains. This means that we have established the adiabatic topological passages assisted by the zero energy state that can be used for controllable quantum information transfer, where the giant atom acts as the signal transmitter and the ends of the two SSH chains (A_1, B_{2N}, C_1, D_{2N}) act as information receivers. The information transfer to the leftmost or rightmost end of the two SSH chains is achieved by choosing the coupling points of the giant atom to the SSH chains, and the final probability occupancy is controlled by the coupling ratio g_2/g_1 .

We now confirm the validity of the adiabatic topological passage by directly employing the evolution results of the Hamiltonian (1) with slow time-varying rates, using $N = 4$ as an example. We consider the system is initially in the state $|\psi_i\rangle = |0, \dots, 1_{\text{atom}}, \dots, 0\rangle$, in which the giant atom is in the excited state and the two topological chains are in the vacuum state. We choose the two cases discussed in Fig. 6 for $p = q = 1$ with either $g_1 = g_2 = 0.01J$ or $g_1 = 0.01J, g_2 = 0.02J$. With Schrödinger equation, we can derive the final state $|\psi_f\rangle$. The results of the numerical simulations are displayed in Figs. 8(a) and (b), where $|\psi_{A,1}|^2 (|\psi_{C,1}|^2)$ and $|\psi_{B,2N}|^2 (|\psi_{D,2N}|^2)$ are the probabilities of the leftmost and rightmost sublattices of the SSH-1 chain (SSH-2 chain), respectively. We can see the giant atomic excitation gradually transfers to the rightmost sublattice of the SSH-1 chain B_{2N} and the leftmost sublattice of the SSH-2 chain D_{2N} by adiabatic evolution with $\Omega = 0.0001J$. Furthermore, the results obtained from time-dependent Hamiltonian (1) are consistent with Figs. 4(c) and (d) and Figs. 6(b) and (d), which proves that our previous discussions in the subspace are correct, namely the adiabatic topological passages exist. We also study the adiabatic evolution for $N = 10$, the results are shown in Figs. 8(c) and (d). It can be found that for $N = 10$, it is still possible to realize the transfer of atomic excitations to the ends of two SSH chains.

IV. IMPERFECTIONS

In this section, we discuss the effect of certain imperfections on the adiabatic topological passages. We first discuss the implications of SSH chain-coupled disorder for the adiabatic topological passage. Here there will be two types of disorders. One comes from the disorders of the lattice frequencies, e.g., $(\omega_o + \delta\omega_j)a_j^\dagger a_j$ and $(\omega_o + \delta\omega_j)b_j^\dagger b_j$, another one is from the disorder couplings between lattices, e.g., $(J_1 + \eta_j)a_j^\dagger b_j$ and $(J_2 + \eta_j)a_{j+1}^\dagger b_j$. We consider $\delta\omega_j$ and η_j to be random numbers in the range $[-\xi, \xi]$,

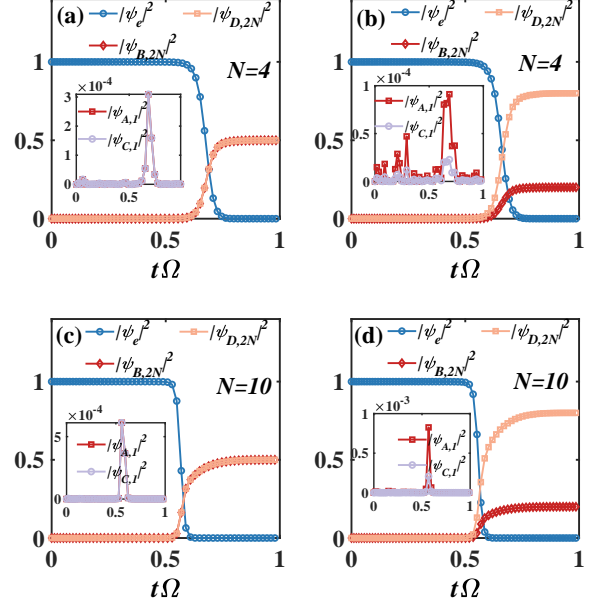


FIG. 8. [(a)-(d)] The probability evolution of the atomic excited state $|\psi_e|^2$, sublattice A_1 ($|\psi_{A,1}|^2$), sublattice B_{2N} ($|\psi_{B,2N}|^2$), sublattice C_1 ($|\psi_{C,1}|^2$) and sublattice D_{2N} ($|\psi_{D,2N}|^2$) versus the time for the giant atom coupled to the sublattice A_1 and C_1 with $\Omega = 10^{-4}J$ and $g_1 = g_2 = 0.01J$ for panels [(a), (c)], $g_1 = 0.01J, g_2 = 0.02J$ for panels [(b), (d)]. The parameters are set to $J = 1$, $N = 4$ for panels [(a), (b)], $N = 10$ for panels [(c), (d)].

where ξ is the disorder strength. In Figs. 9(a) and (b), we plot the effect of frequency disorder with $\xi = 0.001J$ and coupling disorder with $\xi = 0.1J$ on the probability distribution of zero-energy state, respectively. We can see that the adiabatic topological passage is very sensitive to the frequency disorder and robust to the coupling disorder. This is because the edge states of SSH chains are not affected by coupling disorder as long as the disorder strength does not cause a topological phase transition, but are extremely sensitive to frequency disorder.

In Sec. III, we study the resonant interaction between the giant atom and SSH chains with $\Delta = 0$. However, the non-resonant interaction with $\Delta \neq 0$ is also very important. Let us now consider a target state $|\psi_t\rangle = (|0, \dots, 1, 0_{\text{atom}}, 0, \dots, 0, 0\rangle + |0, \dots, 0, 0_{\text{atom}}, 0, \dots, 0, 1\rangle)/\sqrt{2}$, which refers to the superposition of the rightmost lattices B_{2N} and D_{2N} at their excited states for the two SSH chains. This state can be obtained with an evolution time $t_f = \pi/\Omega$ for the resonant interaction between the giant atom and the SSH chains when the giant atom is initially in the excited state and the two topological chains are in their vacuum states. However, in the non-resonant case, the state $|\psi_f\rangle$ at the time $t_f = \pi/\Omega$ is different from the state $|\psi_t\rangle$. The variation of the fidelity $F = \langle \psi_t | \psi_f \rangle$ with Δ is plotted in Fig. 9(c). We can see that for $|\Delta| < 0.15J$, the fidelity

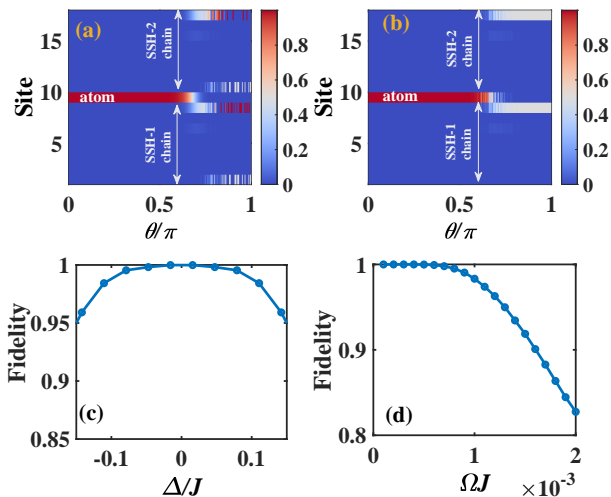


FIG. 9. The probability distribution of zero-energy state on the sites varies with θ for the disorders of the lattice frequencies within the region $\delta\omega_j \in [-0.001J, 0.001J]$ in (a) and the disorder couplings between lattices with $\eta_j \in [-0.001J, 0.001J]$ in (b), respectively. (c) and (d) At time $t_f = \pi/\Omega$, the fidelity varies with Δ and Ω , respectively. The parameters are set to $J = 1$, $N = 4$ for panels [(a-d)], $\Delta = 0$ for panels [(a),(b), (d)], $\Omega = 10^{-4}$ for panel (c).

is greater than 95%, but the fidelity decreases rapidly as the increase of Δ . This is due to the fact that when the detuning Δ is large, the giant atom no longer resonates with the band gap states of the SSH chains, see Eqs. (5) and (6), the fidelity decreases rapidly. Thus, the adiabatic topological passage is immune to weak coupling disorders and very small frequency mismatch between the giant atom and the edge states of the SSH chains.

V. DISCUSSION

We now discuss the experimental feasibility. In recent years, based on the design flexibility and parameter controllability of the system structure [63–66], superconducting quantum circuits have attracted much attention and become into a well-established platform for the study of quantum simulation [67–69] and quantum information processing [70–72]. Recently, the works [73–77] have theoretically and experimentally shown that superconducting quantum circuits can be used to simulate the SSH model, where each cell of the SSH chain can be simulated by either two LC resonators or qubits. Moreover, the periodic modulation of the coupling can also be realized [78, 79]. Therefore, the SSH chains may be realized by superconducting quantum circuits.

The superconducting qubit circuits acting as the giant atoms have been experimentally demonstrated [42–44]. We know that the giant atom inevitably interacts with the environment which results in the loss of the coherence, thus the adiabatic evolution time t_f required to complete the transfer of atomic excitations to the ends of the two SSH chains must be less than the atomic decoherence time. Recently, coherence times from several tens of microseconds to milliseconds ($t \approx 10^{-3}$ s) for superconducting qubits have been demonstrated based on the state-of-the-art experimental systems [80]. In [75], the coupling strength of the SSH chain can be about $J \approx 10^8$ Hz, and thus the time to complete the adiabatic state transfer in our system is about $t_f = \pi/(\Omega J) = 10^{-4}$ s, which is less than the decoherence time of the superconducting qubits. We also plot the fidelity defined in Sec. IV at the time $t_f = \pi/\Omega$ varying with Ω as shown in Fig. 9(d). It can be seen that high fidelity can still be achieved even with a low evolution speed $\Omega J = 10^{-3}$ corresponding to the evolution time $t_f = 10^{-5}$ s. Thus our proposal may be observed in the experiments.

VI. CONCLUSION

We propose an approach to construct an adiabatic topological passage by coupling a giant atom to two SSH chains. The adiabatic topological passage allows the excitation of the giant atom to be delivered in a controllable way to both ends of the two SSH chains. When two finite SSH chains are in the topological phase and the giant atom resonates with the edge states of the SSH chain, the system is reduced to the coupling of the giant atom to the edge states of the two SSH chains. Then the system is equivalent to a five-state model, which includes the edge states of the two SSH chains as well as the giant atom. In this case, we find the presence of dark states in the subspace, which can be worked as an adiabatic topological passage. In this way, we can use adiabatic evolution to transfer the excitation of the giant atom to one end of the two SSH chains in a fully controllable way. In addition, we also show the robustness of the adiabatic topological passage to the coupling disorders in SSH chains and the frequency mismatch between the giant atom and edge states of the SSH chains. Our study may be realized by the superconducting quantum circuits.

VII. ACKNOWLEDGMENTS

This work was supported by the National Natural Science Foundation of China Grants No. 12374483, No.12274053 and No. 92365209.

[1] H. J. Kimble, *Nature* **453**, 1023 (2008).

[2] J. I. Cirac, P. Zoller, H. J. Kimble, and H. Mabuchi, *Phys. Rev. Lett.* **78**, 3221 (1997).

- [3] Y.-A. Chen, S. Nascimbène, M. Aidelsburger, M. Atala, S. Trotzky, and I. Bloch, *Phys. Rev. Lett.* **107**, 210405 (2011).
- [4] A. Reiserer and G. Rempe, *Rev. Mod. Phys.* **87**, 1379 (2015).
- [5] S. Ritter, C. Nölleke, C. Hahn, A. Reiserer, A. Neuzner, M. Uphoff, M. Mücke, E. Figueroa, J. Bochmann, and G. Rempe, *Nature* **484**, 195 (2012).
- [6] B. Vermersch, P.-O. Guimond, H. Pichler, and P. Zoller, *Phys. Rev. Lett.* **118**, 133601 (2017).
- [7] M. C. Kuzyk and H. Wang, *Phys. Rev. X* **8**, 041027 (2018).
- [8] C. J. Axline, L. D. Burkhardt, W. Pfaff, M. Zhang, K. Chou, P. Campagne-Ibarcq, P. Reinhold, L. Frunzio, S. M. Girvin, L. Jiang, M. H. Devoret, and R. J. Schoelkopf, *Nature Physics* **14**, 705 (2018).
- [9] F. Mei, G. Chen, L. Tian, S.-L. Zhu, and S. Jia, *Phys. Rev. A* **98**, 012331 (2018).
- [10] D. Petrosyan and P. Lambropoulos, *Opt. Commun.* **264**, 419 (2006), quantum Control of Light and Matter.
- [11] N. V. Vitanov, A. A. Rangelov, B. W. Shore, and K. Bergmann, *Rev. Mod. Phys.* **89**, 015006 (2017).
- [12] J. R. Kuklinski, U. Gaubatz, F. T. Hioe, and K. Bergmann, *Phys. Rev. A* **40**, 6741 (1989).
- [13] K. Bergmann, H. Theuer, and B. W. Shore, *Rev. Mod. Phys.* **70**, 1003 (1998).
- [14] B. Chen, W. Fan, Y. Xu, Y.-D. Peng, and H.-Y. Zhang, *Phys. Rev. A* **88**, 022323 (2013).
- [15] M. Z. Hasan and C. L. Kane, *Rev. Mod. Phys.* **82**, 3045 (2010).
- [16] L. A. Wray, S. Y. Xu, Y. Xia, Y. S. Hor, D. Qian, A. V. Fedorov, H. Lin, A. Bansil, R. J. Cava, and M. Z. Hasan, *Nat. Phys.* **6**, 855 (2010).
- [17] M. I. Shalaev, W. Walasik, A. Tsukernik, Y. Xu, and N. M. Litchinitser, *Nat. Nanotechnol.* **14**, 31 (2019).
- [18] T. Ozawa, H. M. Price, A. Amo, N. Goldman, M. Hafezi, L. Lu, M. C. Rechtsman, D. Schuster, J. Simon, O. Zeitlinger, and I. Carusotto, *Rev. Mod. Phys.* **91**, 015006 (2019).
- [19] D. J. Thouless, *Phys. Rev. B* **27**, 6083 (1983).
- [20] Y. E. Kraus, Y. Lahini, Z. Ringel, M. Verbin, and O. Zeitlinger, *Phys. Rev. Lett.* **109**, 106402 (2012).
- [21] S. Longhi, G. L. Giorgi, and R. Zambrini, *Adv. Quantum Technol.* **2**, 1800090 (2019).
- [22] N. E. Palaiodimopoulos, I. Brouzos, F. K. Diakonov, and G. Theocharis, *Phys. Rev. A* **103**, 052409 (2021).
- [23] S. Longhi, *Phys. Rev. B* **99**, 155150 (2019).
- [24] F. M. D'Angelis, F. A. Pinheiro, D. Guéry-Odelin, S. Longhi, and F. m. c. Impens, *Phys. Rev. Res.* **2**, 033475 (2020).
- [25] T. Tian, Y. Zhang, L. Zhang, L. Wu, S. Lin, J. Zhou, C.-K. Duan, J.-H. Jiang, and J. Du, *Phys. Rev. Lett.* **129**, 215901 (2022).
- [26] D.-W. Wang, C. Zhao, J. Yang, Y.-T. Yan, and L. Zhou, *Phys. Rev. A* **107**, 053701 (2023).
- [27] C. Wang, L. Li, J. Gong, and Y. X. Liu, *Phys. Rev. A* **106**, 052411 (2022).
- [28] L. Qi, G.-L. Wang, S. Liu, S. Zhang, and H.-F. Wang, *Phys. Rev. A* **102**, 022404 (2020).
- [29] J. Cao, W.-X. Cui, X. X. Yi, and H.-F. Wang, *Phys. Rev. A* **103**, 023504 (2021).
- [30] L.-N. Zheng, X. Yi, and H.-F. Wang, *Phys. Rev. Appl.* **18**, 054037 (2022).
- [31] L. Qi, N. Han, S. Liu, H.-F. Wang, and A.-L. He, *Phys. Rev. A* **107**, 062214 (2023).
- [32] L. Qi, Y. Yan, Y. Xing, X.-D. Zhao, S. Liu, W.-X. Cui, X. Han, S. Zhang, and H.-F. Wang, *Phys. Rev. Res.* **3**, 023037 (2021).
- [33] L. Qi, Y. Xing, X.-D. Zhao, S. Liu, S. Zhang, S. Hu, and H.-F. Wang, *Phys. Rev. B* **103**, 085129 (2021).
- [34] M. Ezawa, *Phys. Rev. B* **109**, 205421 (2024).
- [35] W. Nie, Z. H. Peng, F. Nori, and Y. X. Liu, *Phys. Rev. Lett.* **124**, 023603 (2020).
- [36] W. Nie and Y. X. Liu, *Phys. Rev. Res.* **2**, 012076 (2020).
- [37] C. Dłaska, B. Vermersch, and P. Zoller, *Quantum Sci. Technol.* **2**, 015001 (2017).
- [38] N. Y. Yao, C. R. Laumann, A. V. Gorshkov, H. Weimer, L. Jiang, J. I. Cirac, P. Zoller, and M. D. Lukin, *Nat. Commun.* **4**, 1585 (2013).
- [39] J. Wei, *Phys. Rev. A* **106**, 033710 (2022).
- [40] C. I. Kvande, D. B. Hill, and D. Blume, *Phys. Rev. A* **108**, 023703 (2023).
- [41] D.-W. Wang, C. Zhao, J. Yang, Y.-T. Yan, and L. Zhou, *Phys. Rev. A* **109**, 033708 (2024).
- [42] G. Andersson, B. Suri, L. Guo, T. Aref, and P. Delsing, *Nat. Phys.* **15**, 1123 (2019).
- [43] B. Kannan, M. J. Ruckriegel, D. L. Campbell, A. Frisk Kockum, J. Braumüller, D. K. Kim, M. Kjaergaard, P. Krantz, A. Melville, B. M. Niedzielski, A. Vepsäläinen, R. Winik, J. L. Yoder, F. Nori, T. P. Orlando, S. Gustavsson, and W. D. Oliver, *Nature* **583**, 775 (2020).
- [44] C. Joshi, F. Yang, and M. Mirhosseini, *Phys. Rev. X* **13**, 021039 (2023).
- [45] A. M. Vadiraj, A. Ask, T. G. McConkey, I. Nsanzineza, C. W. S. Chang, A. F. Kockum, and C. M. Wilson, *Phys. Rev. A* **103**, 023710 (2021).
- [46] A. Frisk Kockum, P. Delsing, and G. Johansson, *Phys. Rev. A* **90**, 013837 (2014).
- [47] P. Y. Wen, K.-T. Lin, A. F. Kockum, B. Suri, H. Ian, J. C. Chen, S. Y. Mao, C. C. Chiu, P. Delsing, F. Nori, G.-D. Lin, and I.-C. Hoi, *Phys. Rev. Lett.* **123**, 233602 (2019).
- [48] A. F. Kockum, G. Johansson, and F. Nori, *Phys. Rev. Lett.* **120**, 140404 (2018).
- [49] A. Carollo, D. Cilluffo, and F. Ciccarello, *Phys. Rev. Res.* **2**, 043184 (2020).
- [50] L. Du, L. Guo, and Y. Li, *Phys. Rev. A* **107**, 023705 (2023).
- [51] A. Soro and A. F. Kockum, *Phys. Rev. A* **105**, 023712 (2022).
- [52] X. Wang, T. Liu, A. F. Kockum, H.-R. Li, and F. Nori, *Phys. Rev. Lett.* **126**, 043602 (2021).
- [53] S. Guo, Y. Wang, T. Purdy, and J. Taylor, *Phys. Rev. A* **102**, 033706 (2020).
- [54] L. Guo, A. F. Kockum, F. Marquardt, and G. Johansson, *Phys. Rev. Res.* **2**, 043014 (2020).
- [55] F. Roccati and D. Cilluffo, *Phys. Rev. Lett.* **133**, 063603 (2024).
- [56] W. Cheng, Z. Wang, and Y. X. Liu, *Phys. Rev. A* **106**, 033522 (2022).
- [57] Y.-T. Chen, L. Du, L. Guo, Z. Wang, Y. Zhang, Y. Li, and J.-H. Wu, *Commun. Phys.* **5**, 215 (2022).
- [58] P. Delplace, D. Ullmo, and G. Montambaux, *Phys. Rev. B* **84**, 195452 (2011).
- [59] J. Zak, *Phys. Rev. Lett.* **62**, 2747 (1989).
- [60] J. K. Asbóth, L. Oroszlány, and A. Pályi, [arXiv:1509.02295](https://arxiv.org/abs/1509.02295).

- [61] N. R. Bernier, L. D. Tóth, A. K. Feofanov, and T. J. Kippenberg, *Phys. Rev. A* **98**, 023841 (2018).
- [62] L. Bai, M. Harder, Y. P. Chen, X. Fan, J. Q. Xiao, and C.-M. Hu, *Phys. Rev. Lett.* **114**, 227201 (2015).
- [63] X. Gu, A. F. Kockum, A. Miranowicz, Y. X. Liu, and F. Nori, *Phys. Rep.* **718-719**, 1 (2017).
- [64] P. Krantz, M. Kjaergaard, F. Yan, T. P. Orlando, S. Gustavsson, and W. D. Oliver, *Appl. Phys. Rev.* **6**, 021318 (2019).
- [65] A. Blais, A. L. Grimsmo, S. M. Girvin, and A. Wallraff, *Rev. Mod. Phys.* **93**, 025005 (2021).
- [66] D. Vion, A. Aassime, A. Cottet, P. Joyez, H. Pothier, C. Urbina, D. Esteve, and M. H. Devoret, *Science* **296**, 886 (2002).
- [67] I. Buluta and F. Nori, *Science* **326**, 108 (2009).
- [68] M. Fitzpatrick, N. M. Sundaresan, A. C. Y. Li, J. Koch, and A. A. Houck, *Phys. Rev. X* **7**, 011016 (2017).
- [69] C. Noh and D. G. Angelakis, *Rep. Prog. Phys.* **80**, 016401 (2016).
- [70] A. J. Daley, I. Bloch, C. Kokail, S. Flannigan, N. Pearson, M. Troyer, and P. Zoller, *Nature* **607**, 667 (2022).
- [71] A. Blais, J. Gambetta, A. Wallraff, D. I. Schuster, S. M. Girvin, M. H. Devoret, and R. J. Schoelkopf, *Phys. Rev. A* **75**, 032329 (2007).
- [72] M. Mirhosseini, E. Kim, X. Zhang, A. Sipahigil, P. B. Dieterle, A. J. Keller, A. Asenjo-Garcia, D. E. Chang, and O. Painter, *Nature* **569**, 692 (2019).
- [73] Z. Tao, W. Huang, J. Niu, L. Zhang, Y. Ke, X. Gu, L. Lin, J. Qiu, X. Sun, X. Yang, J. Zhang, J. Zhang, S. Zhao, Y. Zhou, X. Deng, C. Hu, L. Hu, J. Li, Y. Liu, D. Tan, Y. Xu, T. Yan, Y. Chen, C. Lee, Y. Zhong, S. Liu, and D. Yu, [arXiv:2303.04582](https://arxiv.org/abs/2303.04582).
- [74] X. Gu, S. Chen, and Y. X. Liu, [arXiv:1711.06829](https://arxiv.org/abs/1711.06829).
- [75] E. Kim, X. Zhang, V. S. Ferreira, J. Banker, J. K. Iverson, A. Sipahigil, M. Bello, A. González-Tudela, M. Mirhosseini, and O. Painter, *Phys. Rev. X* **11**, 011015 (2021).
- [76] M. Bello, G. Platero, J. I. Cirac, and A. González-Tudela, *Sci. Adv.* **5**, 1 (2019), 1811.04390.
- [77] L. Leonforte, A. Carollo, and F. Ciccarello, *Phys. Rev. Lett.* **126**, 063601 (2021).
- [78] A. A. Houck, H. E. Türeci, and J. Koch, *Nat. Phys.* **8**, 292 (2012).
- [79] S. Schmidt and J. Koch, *Ann. Phys.* **525**, 395 (2013).
- [80] A. Somoroff, Q. Ficheux, R. A. Mencia, H. Xiong, R. Kuzmin, and V. E. Manucharyan, *Phys. Rev. Lett.* **130**, 267001 (2023).